HHS Public Access

Author manuscript

Angew Chem Int Ed Engl. Author manuscript; available in PMC 2021 May 11.

Published in final edited form as:

Angew Chem Int Ed Engl. 2020 May 11; 59(20): 7871–7880. doi:10.1002/anie.201916204.

Bacterial Autoimmune Drug Metabolism Transforms an Immunomodulator into Structurally and Functionally Divergent Antibiotics

Hyun Bong Park[1,2,9], **Tyler N. Goddard**[1,2,9], **Joonseok Oh**[1,2], **Jaymin Patel**[2,3], **Zheng Wei**[2,4], **Corey E. Perez**[1,2], **Brandon Q. Mercado**[1,5], **Rurun Wang**[6], **Thomas P. Wyche**[6], **Grazia Piizzi**[6], **Richard A. Flavell**[4,7], **Jason M. Crawford**[1,2,8,*]

[1]Department of Chemistry, Yale University, New Haven, CT 06520, USA

[2]Chemical Biology Institute, Yale University, West Haven, CT 06516, USA

[3]Department of Molecular, Cellular, and Developmental Biology, Yale University, New Haven, CT 06520, USA

[4]Department of Immunobiology, Yale University School of Medicine, New Haven, CT 06520, USA

[5]Chemical and Biophysical Instrumentation Center, Yale University, New Haven, CT 06520, USA

[6]Exploratory Science Center, Merck & Co., Inc., Cambridge, MA, USA

[7]Howard Hughes Medical Institute, Yale University School of Medicine, New Haven, CT 06520, USA

[8]Department of Microbial Pathogenesis, Yale School of Medicine, New Haven, CT 06536, USA

[9]These authors contributed equally: Hyun Bong Park, Tyler N. Goddard

Abstract

The stilbene tapinarof is a drug used to treat psoriasis and atopic dermatitis. Efficacy is thought to arise from its regulation of the aryl hydrocarbon receptor and nuclear factor erythroid 2-related factor 2 signaling pathways, which have also been linked to the severity of inflammatory bowel diseases. Tapinarof is produced by the gammaproteobacterial *Photorhabdus* genus, which infects insects and humans. Consequently, *Photorhabdus* represents a model to probe tapinarof structural and functional transformations. Here, we demonstrate that *Photorhabdus* transforms tapinarof into novel drug metabolism products that kill inflammatory bacteria. We show that a cupin contributes to the conversion of tapinarof and related dietary stilbenes into novel dimers. One dimer has activity against MRSA and VRE, whereas another undergoes spontaneous cyclization events to

*Correspondence: jason.crawford@yale.edu.

AUTHOR CONTRIBUTIONS

H.B.P., T.N.G., and J.M.C. conceived and designed experiments. H.B.P. and T.N.G. carried out experiments and analyzed data. J.O. performed computational ECD studies and helped NMR measurement of **4**. J.P. performed and analyzed AhR and Nrf2 assays. Z.W. performed the mouse studies. C.E.P. constructed a mutant of *plu1886*. R.W., T.P.W & G.P. contributed to BioMap analysis of **3** and **4**. B.Q.M. resolved the crystal structure of **4**. R.A.F. conceived and supervised the *in vivo* mouse studies. H.B.P., T.N.G., and J.M.C. wrote the paper, and all authors contributed to editing the paper.

CONFLICT OF INTEREST

R.A.F. is a recipient of a grant from AbbVie Inc.

construct a cyclopropane bridge-containing hexacyclic framework that exhibits activity against *Mycobacterium*. Consistent with the functional transformations, these dimers lack efficacy in a colitis mouse model, whereas the monomer reduces disease symptoms.

Graphical Abstract

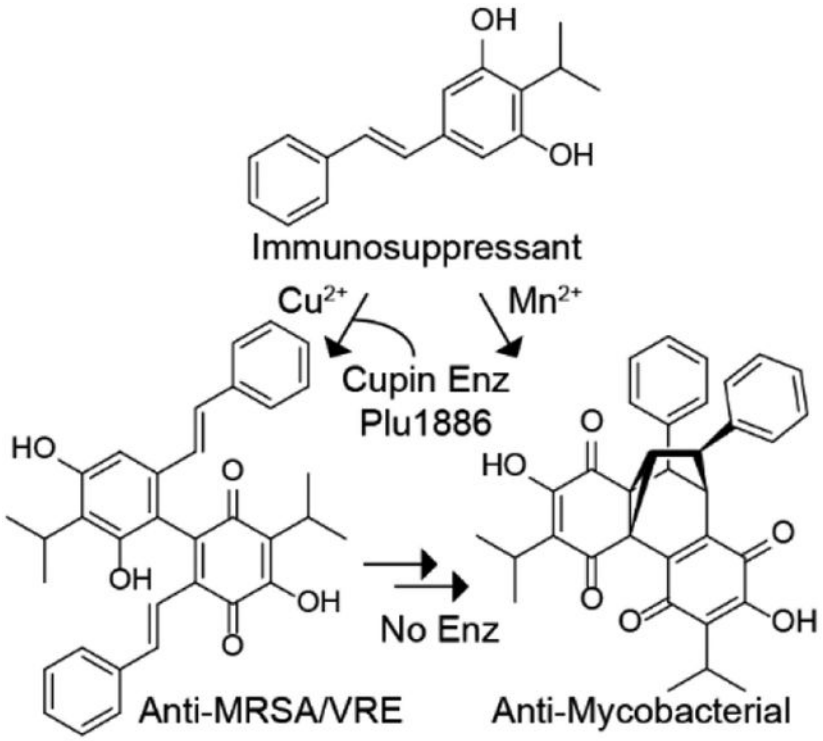

The stilbene tapinarof, a drug used to treat skin inflammatory diseases, is transformed into two novel dimers in *Photorhabdus*. A cupin contributes to the oxidative dimerization of tapinarof and other dietary stilbenes. While tapinarof significantly reduces severe colitis symptoms in a mouse model, the dimers display antimicrobial activities against *Mycobacterium*, MRSA, and VRE.

Keywords

antibiotics; inflammation; microbiome; natural products; Photorhabdus; stilbene

INTRODUCTION

Psoriasis is a chronic autoimmune disease of the skin, and the microbial consortia on our skin and even in our gut contribute to disease severity.[1] Patients with psoriasis have a higher risk of other inflammatory diseases, including psoriatic arthritis and inflammatory bowel disease (IBD).[2] There is a growing understanding of the genetic and molecular bases of psoriasis;[3] however, the disease is currently incurable and its incidence continues to rise, affecting more than 125 million people worldwide.[4] Accordingly, there is a need for new small molecule drugs to extend the therapeutic arsenal for psoriasis treatments and for a better understanding of both the structural and functional drug transformations that take

place. Tapinarof (*a.k.a.*, Benvitimod, **1**) is a topical non-steroidal anti-inflammatory drug (NSAID) that has been approved in China[5] to treat psoriasis and atopic dermatitis.[6] Tapinarof is an isopropyl-substituted stilbene metabolite produced by members of the gammaproteobacterial *Photorhabdus* genus.[7] Recent studies demonstrated that tapinarof activates the aryl hydrocarbon receptor (AhR) signaling program in both human skin cells and mouse models, which is thought to largely account for the drug's clinical efficacy.[8] The AhR is a conserved ligand-dependent transcription factor and is thought to be a key regulator involved in the metabolism of drugs, xenobiotics, and endogenous small molecules.[9] However, it has become clear that the AhR pathway plays important roles in immune signaling in various cell types.[10] Tapinarof has also been shown to activate the nuclear factor erythroid 2-related factor 2 (Nrf2) antioxidant signaling pathway involved in the cellular defense of reactive oxygen species (ROS) and electrophilic cell stress,[8, 11] which is also thought to in part contribute to the drug's clinical efficacy.[8]

Natural stilbenes (1,2-diphenylethylene core), including the dietary supplement resveratrol, are a vast class of phenylpropanoid polyketides commonly found in dietary plants (*e.g.*, grapes, peanuts, blueberries, and others).[12] Plant stilbenes have been used as alternative therapies in the treatment of IBDs[13] and are known to access the bloodstream;[14] however, clinical trials for IBDs ultimately failed due to inter-individual clinical variability.[13, 15] Modifications of stilbene monomers, including glycosylation, prenylation, dimerization, and polymerization, result in enormous overall chemical complexity.[16] Even modest structural modifications can dramatically alter their biological functions.[8, 16] Intriguingly, *Photorhabdus* is a rare bacterial stilbene producer[7a, 17] that convergently evolved an atypical type II PKS route for their biosynthesis,[18] suggesting a selective pressure to generate "plant-type" stilbenes in their ecological niche.

Photorhabdus members are endosymbionts of parasitic nematodes that typically infect diverse insect larvae (entomopathogens).[19] *Photorhabdus asymbiotica* is a pathogen of both insects and occasionally humans, whereas *Photorhabdus luminescens* is limited to insect hosts. *P. asymbiotica* causes severe soft tissue infections of the skin and systemic infections of the bloodstream.[20] Clinical diagnoses of *P. asymbiotica* infections have largely occurred in the United States and Australia,[20–21] although this emerging pathogen is now being recognized worldwide.[22] The bacteria engage in stochastic phase variation – P-form and M-form – to adapt to this multipartite lifecycle, which is regulated by an ON/OFF invertible promoter switch.[23] The pathogenic P-form produces diverse secondary metabolites to modulate the host immune system, promote nematode development, kill microbial competitors, and manage immune-associated oxidative cell stress.[17d, 23c] However, the small colony variant M-form colonizes specific cells in the host nematode intestinal tract to facilitate vertical transmission to nematode progeny.[23a, 23b] Tapinarof (**1**) and related analogs (e.g., **2**-**3**[24]) are produced in the P-form[17b, 23b, 25] and contribute to innate immunosuppression, nematode development, and antioxidant defense.[18b, 26] The metabolites also exhibit modest activity against fungi and Gram-positive bacteria.[17c, 24–25]

Here, we characterized the differential responses of phenylpropanoid-polyetide-derived metabolites **1**-**5** in *P. luminescens* and *P. asymbiotica* to redox cellular stress as a mimetic of host immune stress.[27] By integrating NMR, MS, X-ray crystallography, ECD, and

computational studies, we characterized the structures of novel **4** and **5** as stilbene dimers of tapinarof (**1**). Product **4** featured a complex hexacyclic framework containing a conjugated cyclopropane motif, which we named carbocyclinone-534 (**4**). Product **5**, termed duotap-520, exhibited a resorcinol-benzoquinone C-C bond linkage. We observed that **4** and **5** can form to an extent through spontaneous oxidation and dimerization of **1**; however, an orphan cupin-type enzyme, Plu1886, enhances the regioselective bifurcation of **1** to **5** or **1** to **4** (via an unstable intermediate) *in vitro*, which is differentially affected by select metal cofactor supplements. Relative to tapinarof (**1**), duotap-520 (**5**) exhibited much higher potency against methicillin-resistant *Staphylococcus aureus* (MRSA) and vancomycin-resistant *Enterococcus faecalis* (VRE), whereas carbocyclinone-534 (**4**) possessed growth inhibitory activity against a *Mycobacterial* indicator strain, *M. smegmatis*. Further, duotap (**5**) regulated a reporter gene of Nrf2 in human colon epithelial cells with higher potency than the parent drug. Lastly, in a DSS-colitis mouse model, tapinarof showed a statistically-significant reduction in disease symptoms, whereas the dimers had little to no effect, which was consistent with their functional transformations.

RESULTS AND DISCUSSION

Photorhabdus Metabolites Are Enhanced in Response to Redox Cell Stress.

During infections, bacteria respond to a myriad of cellular stresses derived from the host such as redox stress.[28] *Photorhabdus* pathogenicity is associated with the rich circulatory system of infected hosts.[19a, 29] Thus, we initially challenged *P. luminescens* to redox stress in a nutrient-rich background. Redox stress was induced by supplementation of two sub-inhibitory concentrations (12.5 and 6.25 μM) of paraquat (1,1′-dimethyl-4,4′-bipyridinium dichloride), which generates reactive oxygen species (ROS)[27] (Figure S1), and we aerobically cultivated *P. luminescens* under redox stress conditions at 30 °C until they reached stationary phase (48 h, Figure 1a). Relative to the paraquat-free cultures, extracted ion count (EIC)-based LC-MS data of redox-stressed cultures revealed enhancement of three distinct peaks with complex UV-visible chromophores eluting at t_R = 25.4 (**3**), 26.1 (**4**), and 26.8 (**5**) min (Figure 1a and Figure S1). The high-resolution mass data ($[M+H]^+$ *m/z* 284.1289, 535.2120, and 521.2320) suggested the molecular formulas of **3**, **4**, and **5** to be $C_{17}H_{17}NO_3$, $C_{34}H_{30}O_6$, and $C_{34}H_{32}O_5$, respectively (Figure S2). Through the analysis of UV-visible chromophores corresponding to **3**-**5** and comparison to our prior analysis, we demonstrated that **3** is a previously known amino-substituted tapinarof derivative, lumiquinone A,[24] while **4** and **5** were not consistent with those of previous stilbene-derived metabolites (Figure S2). Since lumiquinone A (**3**) is related to tapinarof, we also analyzed the comparative responses of the two major *Photorhabdus* stilbenes, tapinarof (**1**) and its epoxidation product **2**[17b, 25] (Figure 1a,b). While the production levels of **2** (t_R = 20.7 min) were unaffected, **1** (t_R = 21.6 min) was significantly decreased in a dose-dependent manner, indicating an inverse correlation between **1** and **3**-**5** in their production (Figure 1a,b and Figure S1). In the absence of *P. luminescens*, supplementation of paraquat (12.5 and 6.25 μM) to generate ROS in fresh LB medium containing tapinarof (**1**) did not affect the production level of **4** and **5** (Figure S3).

We next examined the production of these metabolites in two genetically-locked strains of *P. luminescens*, in which the M- and P-forms do not interconvert, to unambiguously evaluate the contributions of bacterial phase variation on metabolite production.[23b] C_{18}-reversed-phase LC-MS analysis of the extracts demonstrated that the entire family of metabolites were only produced in the P-form associated with pathogenesis and that they were undetectable in the M-form cultures (Figure 1c). We also cultivated a clinical isolate of *P. asymbiotica*, and **1**, **3**, and **4** were readily detected, whereas **2** and **5** were below detection limits under the conditions of our small-scale experiments (Figure 1c). A larger-scale culture of *P. asymbiotica* in LB medium led to detectable levels of **5** (Figure S4).

Structural Characterization of Metabolites 4 and 5.

The structure of **4** was fully characterized by extensive interpretation of 1D (^{1}H, ^{13}C, and 1D-NOESY) and 2D (^{1}H-^{1}H gCOSY, ^{1}H-^{13}C gHSQCAD, ^{1}H-^{13}C gHMBCAD, LR-HSQMBC, 1,1-ADEQUATEAD, and ROESYAD) NMR data (Figures S5–S15). As key NMR interpretations, the $^3J_{CH}$ HMBC cross-peaks from a methine H-15 to a ketocarbonyl C-4 and a quaternary carbon C-2 functionalized with a hydroxyl group, and from H-7 to two ketocarbonyls C-1 and C-4 constructed a moiety of 2-hydroxy-3-isopropylcyclohexene-1,4-dione (Figure S9). Similarly, a benzoquinone motif was built by the $^3J_{CH}$ HMBC cross-peaks from H-15′ to C-2′ and C-4′, and from H-7′ to C-1′ and C-5′ (Figure S9). Finally, key HMBC correlations from a methine H-7 to C-1, C-4, C-7′ and C-8′ led to the construction of a complex hexacyclic ring system featuring tricyclo[3.2.1.0^{2,7}]oct-3-ene core in **4** (Figure 2a), which was further supported by an LR-HSQMBC experiment capable of displaying long range heteronuclear correlations (*i.e.*, $^4J_{CH}$ and/or $^5J_{CH}$)[30] (Figure S10). The existence of a cyclopropane motif in **4** was confirmed by the 1,1-ADEQUATEAD ($^1J_{CC}$ = 10 Hz) NMR correlations from a methine proton H-7 to two quaternary carbons C-4 and C-5 (Figure 2a) (Figure S12). Thus, the structure of **4** was characterized to be a novel tapinarof-derived dimer representing a complex hexacyclic framework,[31] which we named carbocyclinone-534 (**4**). The relative structure of **4** was supported by the interpretation of 2D ROESYAD and 1D NOESY combined with an analysis of measured interproton distance (2.3Å) in solution between H-8 and H-8′, using the peak amplitude normalization for improved cross-relaxation (PANIC) method[32] (Figures S13–S15).

The complex structure of **4** prompted us to confirm the NMR-based assignments through X-ray crystallography; **4** was successfully crystallized in a combination of water and acetonitrile (a ratio of 1:1) under slow solvent evaporation at 4 °C. Single crystal X-ray diffraction analysis conducted with Cu Kα radiation (λ = 1.54178 Å) unambiguously supported the absolute structure of **4**, and established **4** as a racemic mixture (Figure 2b, Figure S16 and Tables S3–S4). Consistent with X-ray crystallographic analysis, the ECD spectrum of **4** had no Cotton effects (Figure 2d). Thus, **4** was further purified by chiral phase separation, and the corresponding enantiomers (+)-**4** ([α] +3.5, c 0.01, CH_3OH) and (−)-**4** ([α] −4.7, c 0.01, CH_3OH) were isolated in a ratio of *ca.* 1.2:1 (Figure 2e and Figure S17). The absolute configurations of (+)-**4** and (−)-**4** were finally defined as 5*R*,6*S*,7*R*,8*S*,7′*R*,8′*S* and 5*S*,6*R*,7*S*,8*R*,7′*S*,8′*R*, respectively (Figure 2c), by comparing the experimental and calculated ECD spectra simulated by Gaussian 09 (Figure 2e and Tables S5–S6).

The ^{1}H NMR data of **5** were closely related to those of **1**, suggesting **5** is another type of dimerization product of **1** (Figures S18–S21). Interpretation of 2D-(gCOSY, gHSQCAD, and gHMBCAD) NMR spectra of **5** enabled the construction of two distinctive monomeric partial structures, including a tapinarof and a quinone analogue of tapinarof. The two units were directly connected by a C-C bond linkage, which was evident by key HMBC cross-peaks from H-1 to C-5, and from H-7′ to C-5′, yielding a new heterodimer of tapinarof, which we named duotap-520 (**5**) (Figure 2f). The structure was finally supported by the molecular formula ($C_{34}H_{32}O_5$) deduced from the HR-ESI-QTOF-MS data ($[M+H]^+$ *m/z* 521.2320, calcd 521.2321). Comprehensive analyses of NMR, X-ray crystallography, ECD, and computational data of new molecules **4** and **5** supported them as tapinarof-derived products. Under aerobic conditions, **5** could be slowly converted to **4** spontaneously (Figure S22).

An Orphan Bacterial Cupin Enzyme Enhances Regioselective Dimerization of Tapinarof.

Enzymatic oxidative dimerization of natural stilbenes has previously been described.[33] Given the resorcinol moiety in **1**, we also anticipated that a facile oxidation process could lead to the dimerization of **1** to yield **4** and **5**. To test this, we evaluated the tapinarof biosynthetic gene cluster encoded in the genomes of *P. luminescens* TT01 and *P. asymbiotica*, which is fragmented into at least four regions of the genome.[18b] Using similar genome context, we previously identified a separate clustered gene involved in the stereoselective epoxidation of tapinarof to **2**.[17b] In this study, we focused on gene *plu1886* that encodes a candidate cupin-type enzyme and is located adjacent to *bkdC* (*plu1885*), a ketosynthase that participates in tapinarof biosynthesis.[18b] Genome synteny analysis revealed that Plu1886 is conserved in *Photorhabdus* species including *P. asymbiotica* (Figure 3a). Proteins in the cupin superfamily are widespread in plants and are known to catalyze diverse oxidation reactions.[34]

To establish function of Plu1886 *in vitro*, we cloned, overexpressed, and purified an N-terminal His_6-tagged-Plu1886 variant (Table S7 and Figure S23). Because oxidative cupin enzymes frequently use metal ions to catalyze reactions, we tested eight different metal supplements (Ni^{2+}, Ca^{2+}, Fe^{2+}, Cu^{2+}, Zn^{2+}, Co^{2+}, Mg^{2+}, and Mn^{2+}) at 1 mM for their effects on the *in vitro* activity of Plu1886. EIC analysis of the reactions demonstrated conversion of substrate **1** into **4** and **5** in the presence of various metals, with highest production of **4** in the presence of Mn^{2+} and of **5** in the presence of Cu^{2+} (Figure 3b,c). The ECD spectrum of purified enzyme-derived product **4** also showed no Cotton effects, which is consistent with the naturally isolated racemic mixture of **4** (Figure S24). Spontaneous production of **4** and **5** also occurs to an extent in the presence of metal supplements under the conditions of our experiments, and we observed enzyme-dependent enhancements of these dimerization reactions (Figure 3e, f, and see below). Product **5** was prepared at earlier incubation times (2 h incubation shown), while **4** accumulated only at later time points (overnight incubation shown), suggesting that **5** is the intended product. Presence of the cupin protein appears to bifurcate regioselective dimerization of **1** to **4** or **1** to **5** in a redox-active metal-dependent manner. In addition, we generated a marker-less gene deletion of *plu1886* in wild-type *P. luminescens* using allelic-exchange mutagenesis and compared production levels against its wild-type parent under aerobic and microaerobic culture

conditions. While under aerobic conditions we did not observe differential production of **4** due to spontaneous background production, we observed a significant decrease in the *Δplu1886* strain relative to wild-type under microaerobic culture conditions (Figure 3d). These cellular studies of tapinarof dimerization are consistent with our *in vitro* protein biochemical studies and further support spontaneous background dimerization of **1**, which is enhanced by Plu1886.

The Bacterial Cupin Enzyme Can Utilize Plant Stilbenes as Substrates.

To assess the substrate preferences for Plu1886 in Mn^{2+} or Cu^{2+} supplemented buffers, we analyzed four representative plant-derived stilbenes, reseveratrol (**6**), pinosylvin (**7**), piceatannol (**8**), and chiricanine A (**9**), that served to represent the most common functionalizations of the 1,2-diphenylethylene stilbene core (Figure 4a). We established that both resveratrol (**6**) and pinosylvin (**7**) are competent substrates of cupin Plu1886. Indeed, the cupin robustly converted resveratrol (**6**) to its new carbocyclinone (**6a**) scaffold (Figure 4b) in the Mn^{2+} supplemented buffer, and only trace levels of this metabolite could be detected in the Mn^{2+} supplemented buffer control. For pinosylvin (**7**), we observed robust production of its novel duotap scaffold (**7a**) in the enzyme-catalyzed reaction in the presence of Cu^{2+}, and even trace levels of potential spontaneous **7a** formation were undetectable in any of our control studies (Figure 4c), further supporting the enzyme's dimerization role. The new enzyme-derived products **6a** and **7a** were purified and structurally confirmed by 2D NMR experiments (Figures S25–S32). We did not observe duotap production from **6** or carbocyclinone production from **7** in our enzyme reactions, and we did not detect any derivatives corresponding to dimerization of **8** or **9**, providing structure-activity relationships for Plu1886 among the common plant stilbenes.

Proposed Biosynthesis for the Formation of Metabolites 4 and 5.

Based on the structural and protein biochemical studies, we propose formation of **4** and **5** from **1** via an oxidative dearomatization route (Figure 5). Consistent with cupin biochemistry,[35] a hydrogen atom could be abstracted from the resorcinol ring in **1** to form a semiquinone radical, which could undergo a peroxidation sequence in the presence of molecular oxygen. Molecular oxygen utilization is consistent with our aerobic and microaerobic genetics studies. Peroxide decomposition to **1a** followed by dimerization with a second equivalent of **1a** could construct the unstable homodimeric benzoquinone intermediate **5a**, which was not detected in our screens. This putative intermediate could undergo a spontaneous facile electrocyclization followed by a Diels Alder cyclization to set the cyclopropane ring, leading to the final racemic product **4**. In contrast, coupling of monomers **1** and **1a** could yield heterodimeric **5**, which can slowly oxidize spontaneously to **4** via **5a** (Figure 5). This latter spontaneous oxidation process is analogous to those proposed in the formation of homodimericin[36] and epicolactone.[37] Of note, **5** was not a substrate of Plu1886 in the formation of **4** (Figure S33).

Tapinarof-Derived Products Activate the Expression of Nrf2 and Exhibit Divergent Antibiosis.

To examine if tapinarof and its biotransformation products activate genes associated with the AhR and Nrf2 signaling pathways, we cultured human HCT116 colon cells in the presence of **1**-**5** at varying concentrations. Total RNA was harvested, and qRT-PCR was used to assess relative transcript levels of *cyp1a1* and *nqo1*, genes downstream in the AhR and Nrf2 signaling pathways, respectively. Treatment of cells with **2**-**5** activated the AhR pathway at 10 μM, which was less active than the parent drug **1** (Figure 6a). However, product **5** activated the antioxidant Nrf2 signaling pathway gene more robustly than parent drug **1** (Figure 6b). Because **4** and **5** can be produced spontaneously, enzymatically, and in blood agar (Figure S34), we speculate that these drug metabolism trajectories might impact the clinical efficacy of tapinarof.

Tapinarof has previously been shown to weakly inhibit the growth of a panel of microorganisms, including Gram-positive bacteria. Thus, we evaluated antimicrobial activities of **1**-**5** on two antibiotic-resistant human pathogens, methicillin-resistant *Staphylococcus aureus* (MRSA) and vancomycin-resistant *Enterococcus faecalis* (VRE) using the minimum inhibitory concentration (MIC) method. The MIC values of tapinarof **1** against these pathogens were 50.5 and 27.0 μM, whereas the MIC values of dimer **5** were considerably more potent at 6.5 μM and 4.1 μM against VRE and MRSA, respectively (Figure 6 and Figure S35). However, activity of **4** was attenuated in these assays, and **2** and **3** similarly showed little to no activity (Figure 6 and Figure S35). We next examined the antimycobacterial activities of **1**, **4**, and **5**. Zone of inhibition analysis using an agar disk diffusion assay with a concentration of 100 μg/disk demonstrated that **4** inhibits the growth of *Mycobacterium smegmatis* at a similar level as **1**, whereas **5** was conversely much less active (Figure 6e). These data indicate that the metal-dependent cupin bifurcation of **1** to **4** or **5**, not only dictates alternative structural paths, but also controls alternative functional outcomes. The much stronger antimicrobial activity of **5** relative to tapinarof could in principle more profoundly alter the microbiome composition.

Given the atypical structure of **4**, we further evaluated this compound against a panel of 12 human primary cell-based co-culture systems, including venular endothelial cells, lung fibroblasts, and peripheral blood mononuclear cells (PBMCs), that model several tissues and disease states (BioMAP® Phenotypic Profiling Assay) (Figure 6f). As a key result from this panel, **4** caused a decrease in protein biomarkers P-Selectin, Eotaxin-3, $sPGE_2$, and VCAM-1 in several cell systems, indicating that **4** is anti-inflammatory. The effect of **4** was particularly prominent in the cell system of PBMCs + B cells (BT) with a decrease in all of the biomarkers in this system, most notably secreted immunoglobulin (sIgG).

We lastly investigated whether tapinarof (**1**) and its dimer products (**4** and **5**) could reduce severe colitis symptoms *in vivo* in a colitis mouse model (Figure 7). Dextran sodium sulfate (DSS, 2.5%) was administered for 5 days followed by regular drinking water for an additional 3 days, and pure compounds (5 mg/kg in 10% DMSO) were fed daily to each mouse group from day-1 (D-1) to day 7 (D7) (Figure 7a). Body weights were measured daily from DSS administration, and clinical scores and colon lengths were measured on day

8 (D8). Compared to DMSO vehicle control, the loss of body weight of the mice administered with tapinarof (**1**) was slightly reduced, consistent with a positive treatment effect (Figure 7b and Figure S36). Indeed, groups treated with **1** revealed lower clinical scores in comparison to the DMSO control group (Figure 7c), and the colon length of mice treated with **1** was observed to be longer than that of the control group, again consistent with a positive treatment effect (Figure 7d). Of the three disease symptoms measured, product **5** only showed a modest improvement in clinical score, whereas **4** showed no effect in the mouse model under the conditions of our study. Oxygen becomes more available at the gut host-bacteria interface,[38] and these small molecule-mouse model studies suggest that oxidative dimerization of tapinarof could reduce IBD treatment effects.

CONCLUSIONS

Pathogens of the skin may represent a source of molecules that could serve as leads for the treatment of skin diseases. *P. asymbiotica* causes bloodstream and severe soft tissue infections in humans, including the skin, and all known *Photorhabdus* members produce tapinarof, an immunosuppressant drug used for the treatment of atopic dermatitis and the autoimmune skin disease psoriasis. We demonstrate that *Photorhabdus* in the presence of paraquat stress regulates the differential production of tapinarof and its metabolism products – two novel tapinarof dimers **4** and **5**. While these products can be formed spontaneously in aerobic conditions over long incubation periods, we show that a conserved cupin-type protein Plu1886 enhances the regioselective dimerization of tapinarof leading to **4** and **5**, depending on supplemented metals. Relative to tapinarof, its metabolism product **5** exhibited significantly higher inhibitory activity against multi-drug resistant (MDR) strains, including the common skin pathogen MRSA, whereas product **4** maintained comparable antimycobacterial activity. We further support that these products contribute to cellular phenotypes previously associated with clinical efficacy, including the activation of human AhR and Nrf2 reporter genes. In our cell-based assays, duotap (**5**) showed stronger activity than tapinarof in its ability to regulate the Nrf2 antioxidant reporter gene *nqo1* (free-radical scavenging activity of **5** was not detected using the 1,3-diphenyl-1-picrylhydrazyl assay with concentrations up to 100 μM, Figure S37). We further show that the tapinarof metabolism product **4** has immunomodulatory activities across diverse human cell systems. Similar to the functional drug transformations observed here, the composition of the microbiome could in principle be affected by the antimicrobial tapinarof transformation products with Gram-positive (MRSA and VRE) and *Mycobacterial* activities. By extension, we hypothesize that select microbiome members (*e.g.*, the occasional skin pathogen *P. asymbiotica*) could regulate the direction and extent of these transformations, which would be subject to inter-individual microbiome variability. Indeed, we identified homologous cupin domain-containing enzymes in the human microbiome, which serve as candidates for such transformations that require further study (Figure S38). Based on our observations, analogous reactions could be expected of dietary stilbenes in the gut, and, in principle, the structures and functions of those metabolism products could underlie the inter-individual variability previously observed for stilbenes in IBD clinical trials.[13–15] We note that both Nrf2 and AhR activation, phenotypes observed in our studies, were recently shown to be protective against IBD symptoms in ulcerative colitis mouse models.[39] Our model studies

here on tapinarof provide a molecular foundation for deciphering the broader functional host-microbe-stilbene metabolic axes in the gut and on the skin in future studies.

Supplementary Material

Refer to Web version on PubMed Central for supplementary material.

ACKNOWLEDGMENTS

This work was supported by the National Institutes of Health (1DP2-CA186575 and R00-GM097096), the Burroughs Wellcome Fund (1016720), and the Camille & Henry Dreyfus Foundation (TC-17-011). T.N.G. was in part supported by the National Institutes of Health (5T32GM06754 3-12)

REFERENCES

[1]. a)Zhernakova A, Withoff S, Wijmenga C, Nat. Rev. Endocrinol 2013, 9, 646; [PubMed: 23959365] b)Greb JE, Goldminz AM, Elder JT, Lebwohl MG, Gladman DD, Wu JJ, Mehta NN, Finlay AY, Gottlieb AB, Nat. Rev. Dis. Primers 2016, 2, 16082. [PubMed: 27883001]

[2]. a)Ritchlin CT, Colbert RA, Gladman DD, Engl N. J. Med 2017, 376, 957–970;b)Fu Y, Lee CH, Chi CC, JAMA Dermatol. 2018, 154, 1417–1423. [PubMed: 30422277]

[3]. a)Bowcock AM, Krueger JG, Nat. Rev. Immunol 2005, 5, 699; [PubMed: 16138103] b)Guttman-Yassky E, Krueger JG, Lebwohl MG, Exp. Dermatol 2018, 27, 409–417; [PubMed: 28266782] c)Lowes MA, Suárez-Fariñas M, Krueger JG, Annu. Rev. Immunol 2014, 32, 227–255. [PubMed: 24655295]

[4]. Lambert RJ, Pearson J, J. Appl. Microbiol 2000, 88, 784–790. [PubMed: 10792538]

[5]. Furue M, Hashimoto-Hachiya A, Tsuji G, Int. J. Mol. Sci 2019, 20, 5424.

[6]. a)Bissonnette R, Bolduc C, Maari C, Nigen S, Webster JM, Tang L, Lyle M, J. Eur. Acad. Dermatol. Venereol 2012, 26, 1516–1521; [PubMed: 22077962] b)Bissonnette R, Chen G, Bolduc C, Maari C, Lyle M, Tang L, Webster J, Zhou Y, Arch. Dermatol 2010, 146, 446–449; [PubMed: 20404242] c)Bissonnette R, Poulin Y, Zhou Y, Tan J, Hong HC, Webster J, Ip W, Tang L, Lyle M, Br. J. Dermatol 2012, 166, 853–860. [PubMed: 22182053]

[7]. a)Paul VJ, Frautschy S, Fenical W, Nealson KH, J. Chem. Ecol 1981, 7, 589–597; [PubMed: 24420598] b)Richardson WH, Schmidt TM, Nealson KH, Appl. Environ. Microbiol 1988, 54, 1602–1605. [PubMed: 3415225]

[8]. Smith SH, Jayawickreme C, Rickard DJ, Nicodeme E, Bui T, Simmons C, Coquery CM, Neil J, Pryor WM, Mayhew D, Rajpal DK, Creech K, Furst S, Lee J, Wu D, Rastinejad F, Willson TM, Viviani F, Morris DC, Moore JT, Cote-Sierra J, J. Investig. Dermatol 2017, 137, 2110–2119. [PubMed: 28595996]

[9]. Denison MS, Nagy SR, Annu. Rev. Pharmacol. Toxicol 2003, 43, 309–334. [PubMed: 12540743]

[10]. a)Di Meglio P, Duarte João H., Ahlfors H, Owens Nick D. L., Li Y, Villanova F, Tosi I, Hirota K, Nestle Frank O., Mrowietz U, Gilchrist Michael J., Stockinger B, Immunity 2014, 40, 989–1001; [PubMed: 24909886] b)Wheeler MA, Rothhammer V, Quintana FJ, J. Biol. Chem 2017, 292, 12383–12389. [PubMed: 28615443]

[11]. Kobayashi A, Kang M-I, Watai Y, Tong KI, Shibata T, Uchida K, Yamamoto M, Mol. Cell. Biol 2006, 26, 221–229. [PubMed: 16354693]

[12]. Li TL, Spiteller D, Spencer JB, ChemBioChem 2009, 10, 896–901. [PubMed: 19266535]

[13]. Martin DA, Bolling BW, Food. Funct 2015, 6, 1773–1786. [PubMed: 25986932]

[14]. Berman AY, Motechin RA, Wiesenfeld MY, Holz MK, NPJ Precis. Oncol 2017, 1, 35. [PubMed: 28989978]

[15]. Halliwell B, Rafter J, Jenner A, Am. J. Clin. Nutr 2005, 81, 268S–276S. [PubMed: 15640490]

[16]. Shen T, Wang XN, Lou HX, Nat. Prod. Rep 2009, 26, 916–935. [PubMed: 19554241]

[17]. a)Kontnik R, Crawford JM, Clardy J, ACS Chem. Biol 2010, 5, 659–665; [PubMed: 20524642] b)Park HB, Sampathkumar P, Perez CE, Lee JH, Tran J, Bonanno JB, Hallem EA, Almo SC,

Crawford JM, J. Biol. Chem 2017, 292, 6680–6694; [PubMed: 28246174] c)Shi D, An R, Zhang W, Zhang G, Yu Z, Agric J. Food Chem. 2017, 65, 60–65;d)Shi Y-M, Bode HB, Nat. Prod. Rep 2018, 35, 309–335. [PubMed: 29359226]

[18]. a)Fuchs SW, Bozhüyük KAJ, Kresovic D, Grundmann F, Dill V, Brachmann AO, Waterfield NR, Bode HB, Angew. Chem. Int. Ed 2013, 52, 4108–4112;b)Joyce SA, Brachmann AO, Glazer I, Lango L, Schwär G, Clarke DJ, Bode HB, Angew. Chem. Int. Ed 2008, 47, 1942–1945;c)Williams JS, Thomas M, Clarke DJ, Microbiology 2005, 151, 2543–2550; [PubMed: 16079333] d)Mori T, Awakawa T, Shimomura K, Saito Y, Yang D, Morita H, Abe I, Cell. Chem. Biol 2016, 23, 1468–1479. [PubMed: 27866911]

[19]). a)Clarke DJ, Cell. Microbiol 2008, 10, 2159–2167; [PubMed: 18647173] b)Waterfield NR, Ciche T, Clarke D, Annu. Rev. Microbiol 2009, 63, 557–574. [PubMed: 19575559]

[20]. a)Peel MM, Alfredson DA, Gerrard JG, Davis JM, Robson JM, McDougall RJ, Scullie BL, Akhurst RJ, J. Clin. Microbiol 1999, 37, 3647–3653; [PubMed: 10523568] b)Weissfeld AS, Halliday RJ, Simmons DE, Trevino EA, Vance PH, O'Hara CM, Sowers EG, Kern R, Koy RD, Hodde K, Bing M, Lo C, Gerrard J, Vohra R, Harper J, J. Clin. Microbiol 2005, 43, 4152–4155. [PubMed: 16081963]

[21]. a)Gerrard J, Waterfield N, Vohra R, ffrench-Constant R, Microb. Infect 2004, 6, 229–237;b)Gerrard JG, McNevin S, Alfredson D, Forgan-Smith R, Fraser N, Emerg. Infect. Diseases 2003, 9, 251–254. [PubMed: 12603999]

[22]. Hapeshi A, Waterfield NR, in The Molecular Biology of Photorhabdus Bacteria (Ed.: ffrench-Constant RH), Springer International Publishing, Cham, 2017, pp. 159–177.

[23]. a)Somvanshi VS, Kaufmann-Daszczuk B, Kim K.-s., Mallon S, Ciche TA, Mol. Microbiol 2010, 77, 1021–1038; [PubMed: 20572934] b)Somvanshi VS, Sloup RE, Crawford JM, Martin AR, Heidt AJ, Kim KS, Clardy J, Ciche TA, Science 2012, 337, 88–93; [PubMed: 22767929] c)Vizcaino MI, Guo X, Crawford JM, J. Ind. Microbiol. Biotechnol 2014, 41, 285–299. [PubMed: 24127069]

[24]. Park HB, Crawford JM, J. Nat. Prod 2015, 78, 1437–1441. [PubMed: 25988621]

[25]. Hu K, Li J, Li B, Webster JM, Chen G, Bioorg. Med. Chem 2006, 14, 4677–4681. [PubMed: 16644226]

[26]. Eleftherianos I, Boundy S, Joyce SA, Aslam S, Marshall JW, Cox RJ, Simpson TJ, Clarke DJ, ffrench-Constant RH, Reynolds SE, Proc. Natl. Acad. Sci. U.S.A 2007, 104, 2419–2424. [PubMed: 17284598]

[27]. a)Apel K, Hirt H, Annu. Rev. Plant Biol 2004, 55, 373–399; [PubMed: 15377225] b)Dragin N, Smani M, Arnaud-Dabernat S, Dubost C, Moranvillier I, Costet P, Daniel J-Y, Peuchant E, FEBS Lett. 2006, 580, 3845–3852. [PubMed: 16797015]

[28]. Fang FC, Frawley ER, Tapscott T, Vazquez-Torres A, Cell Host Microbe 2016, 20, 133–143. [PubMed: 27512901]

[29]. a)Crawford JM, Kontnik R, Clardy J, Curr. Biol 2010, 20, 69–74; [PubMed: 20022247] b)Tobias NJ, Bode HB, J. Mol. Biol 2019, 431, 4589–4598. [PubMed: 31071325]

[30]. Williamson RT, Buevich AV, Martin GE, Parella T, J. Org. Chem 2014, 79, 3887–3894. [PubMed: 24708226]

[31]. a)Brehm I, Hinneschiedt S, Meier H, Eur. J. Org. Chem 2002, 2002, 3162–3170;b)Brehm I, Meier H, Eur. J. Org. Chem 2001, 2001, 3307–3311.

[32]. Hu H, Krishnamurthy K, J. Magn. Reson 2006, 182, 173–177. [PubMed: 16807015]

[33]. a)Slomczynski D, Nakas JP, Tanenbaum SW, Appl. Environ. Microbiol 1995, 61, 907–912; [PubMed: 16534974] b)Jeandet P, Delaunois B, Conreux A, Donnez D, Nuzzo V, Cordelier S, Clément C, Courot E, BioFactors 2010, 36, 331–341; [PubMed: 20726013] c)Breuil A-C, Adrian M, Pirio N, Meunier P, Bessis R, Jeandet P, Tetrahedron Lett. 1998, 39, 537–540.

[34]. Dunwell JM, Purvis A, Khuri S, Phytochem. 2004, 65, 7–17.

[35]. Funa N, Funabashi M, Yoshimura E, Horinouchi S, J. Biol. Chem 2005, 280, 14514–14523. [PubMed: 15701630]

[36]. Mevers E, Sauri J, Liu Y, Moser A, Ramadhar TR, Varlan M, Williamson RT, Martin GE, Clardy J, J. Am. Chem. Soc 2016, 138, 12324–12327. [PubMed: 27608853]

[37]. Ellerbrock P, Armanino N, Ilg MK, Webster R, Trauner D, Nat. Chem 2015, 7, 879–882. [PubMed: 26492007]

[38]. Carlson-Banning KM, Sperandio V, Curr. Opin. Microbiol 2018, 41, 83–88. [PubMed: 29258058]

[39]. a)Lu M-C, Ji J-A, Jiang Y-L, Chen Z-Y, Yuan Z-W, You Q-D, Jiang Z-Y, Sci. Rep 2016, 6, 26585–26585; [PubMed: 27215610] b)Wang Q, Yang K, Han B, Sheng B, Yin J, Pu A, Li L, Sun L, Yu M, Qiu Y, Xiao W, Yang H, Int. J. Mol. Med 2018, 41, 868–876. [PubMed: 29207040]

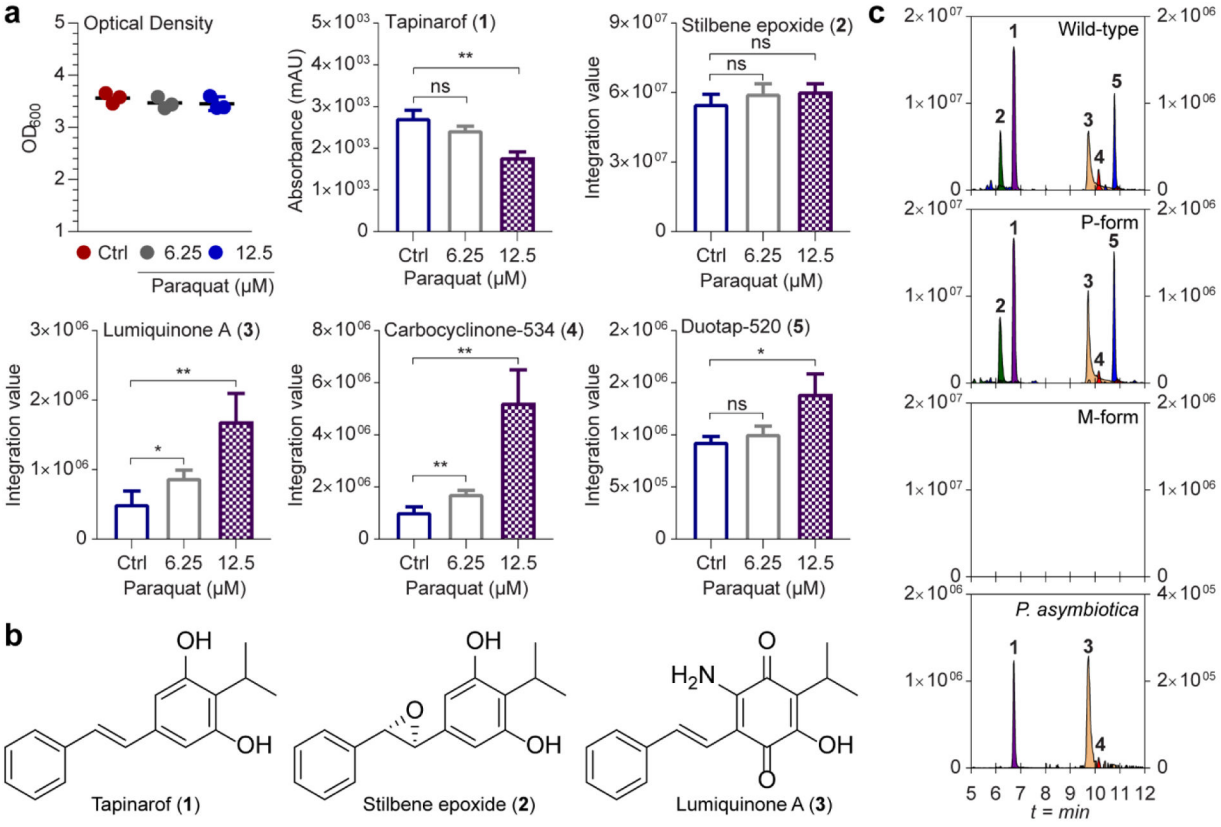

Figure 1. Metabolite profiles of *Photorhabdus* bacteria in response to redox stress.

a, Response of metabolites in *P. luminescens* to paraquat-induced redox stress. Optical densities of cell cultures were measured at 48 h after paraquat exposure compared to controls (Ctrl) lacking paraquat. The *y* axis shows integration values of peaks extracted with corresponding positively charged *m/z* of **1**-**5**. Data are mean ± SEM for three biological replicates. **P* <0.05; ***P* <0.01; ****P* <0.001 by two-tailed student's t-test. ns indicates non-significant. **b**, Structures of tapinarof (**1**), stilbene epoxide (**2**), and lumiquinone A (**3**). **c**, Representative EICs of metabolites **1**-**5** from ethyl acetate-soluble extracts from cultures of *P. luminescens* wild-type (top), genetically locked P- and M-forms (middle), and *P. asymbiotica* (bottom). The scale of *y* axis on the left: relative intensity of **1** and **2**. Right: relative intensity of **3**-**5**. LC/HRMS-QTOF data were analyzed in three independent experiments using a gradient from 50 to 100% aqueous acetonitrile containing 0.1% formic acid over 15 min with a 0.7 ml min^{-1} solvent flow rate.

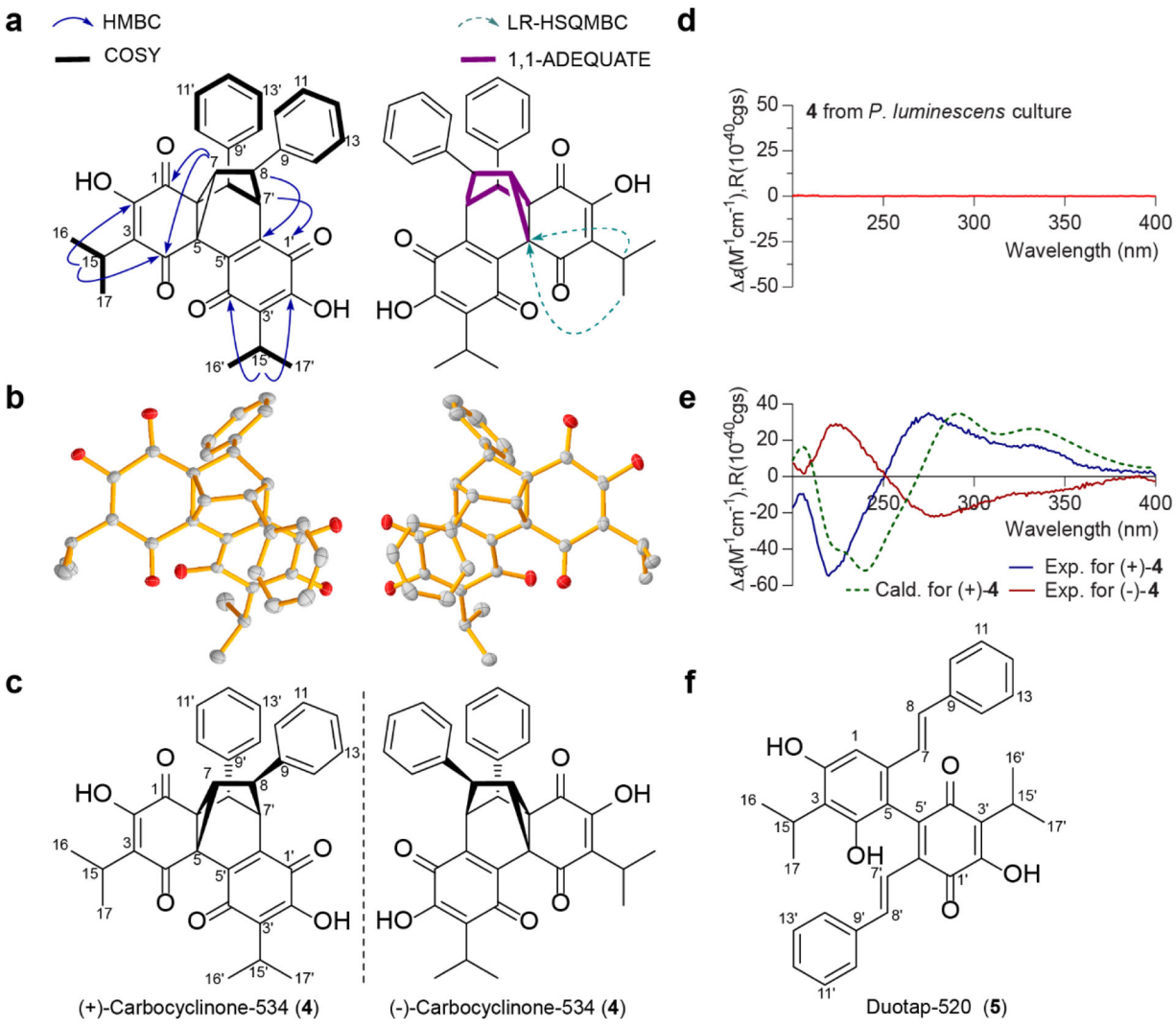

Figure 2. Structural characterization of 4 and 5.

a, Key two-dimensional NMR correlations for the structural assignments of **4**. **b**, ORTEP drawing of X-ray crystal structure of racemic **4**. **c**, A mirror image structure of **4**. **d**, ECD spectrum of **4** isolated from ethyl acetate extracts of *P. luminescens* culture supernatant. **e**, Experimental ECD spectra of optically active **4** purified by chiral-phase chromatography, and ECD comparison of the calculated spectrum of (+)-**4** in methanol at the B3LYP/6–31+G(d,p) level and its experimental spectrum. **f**, Structure of **5**.

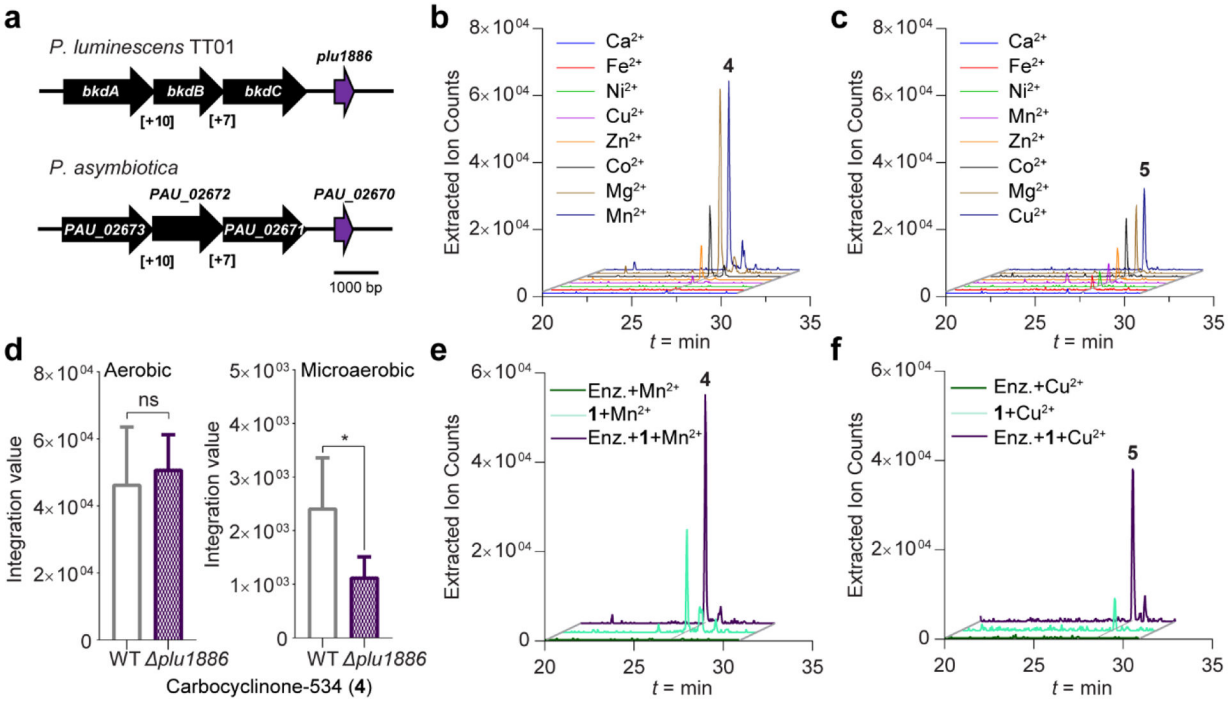

Figure 3. Functional characterization of orphan Plu1886 cupin responsible for the production of 4 and 5 *in vitro*.

a, Annotation of *plu1886* adjacent to known tapinarof biosynthetic genes and synteny with *P. asymbiotica*. **b** and **c**, Extracted ion chromatograms of enzyme reactions showing relative production of **4** and **5** with varying metal ion supplements. **d**, Production of **4** between wild-type *P. luminescens* and *Δplu1886* in aerobic and microaerobic culture conditions. Data are mean ± SEM for six biological replicates. **P* <0.05 by two-tailed student's t-test. ns indicates not-significant. **e** and **f**, Extracted ion counts of *m/z* 535 and 521 corresponding to **4** and **5** from *in vitro* reactions with tapinarof (**1**) in the presence and absence of Plu1886.

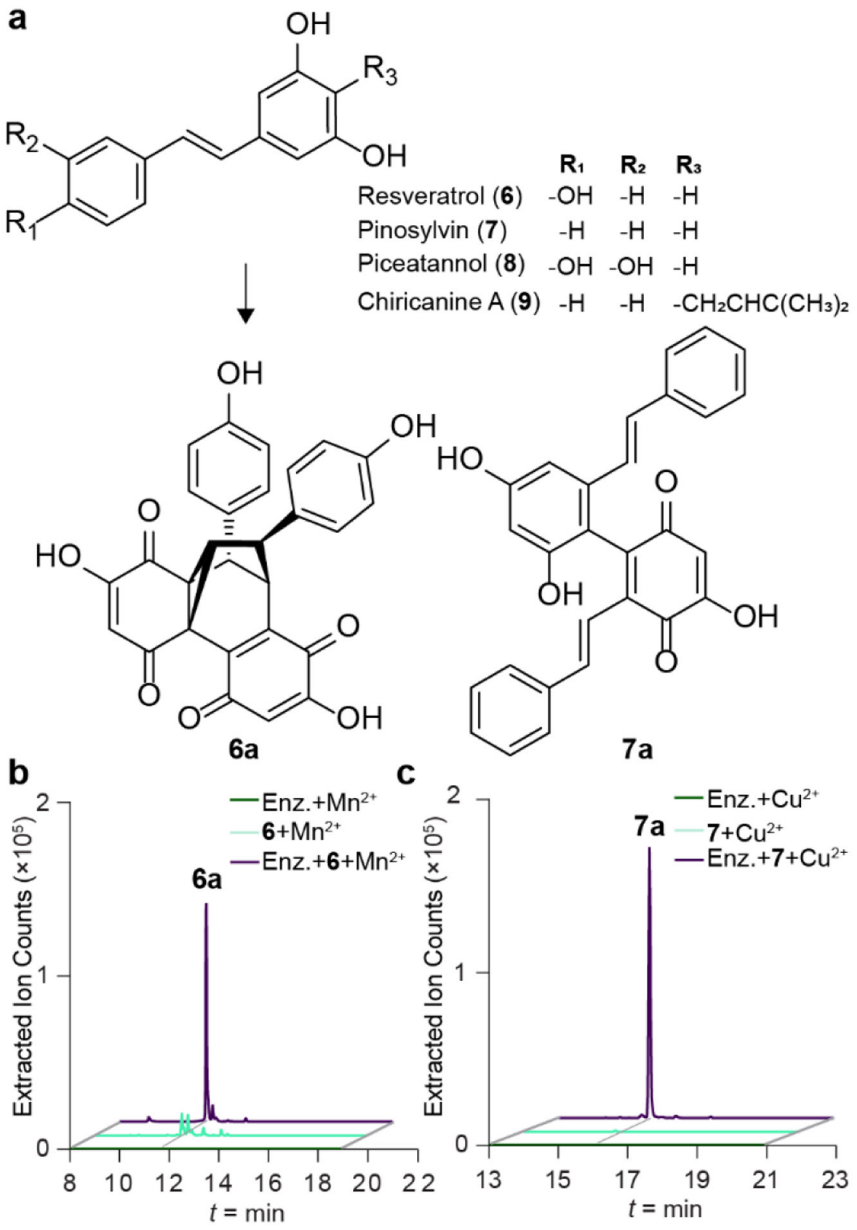

Figure 4. Plu1886-dependent production of carbocyclinone and duotap derivatives from representative plant stilbenes.

a, Plant substrates and enzyme products carbocyclinone-482 (**6a**) and duotap-436 (**7a**) from **6** and **7**. **b** and **c**, Extracted ion counts of *m/z* 483.1080 and 437.1389 corresponding to **6a** and **7a** from *in vitro* reactions with **6** or **7** in the presence and absence of Plu1886.

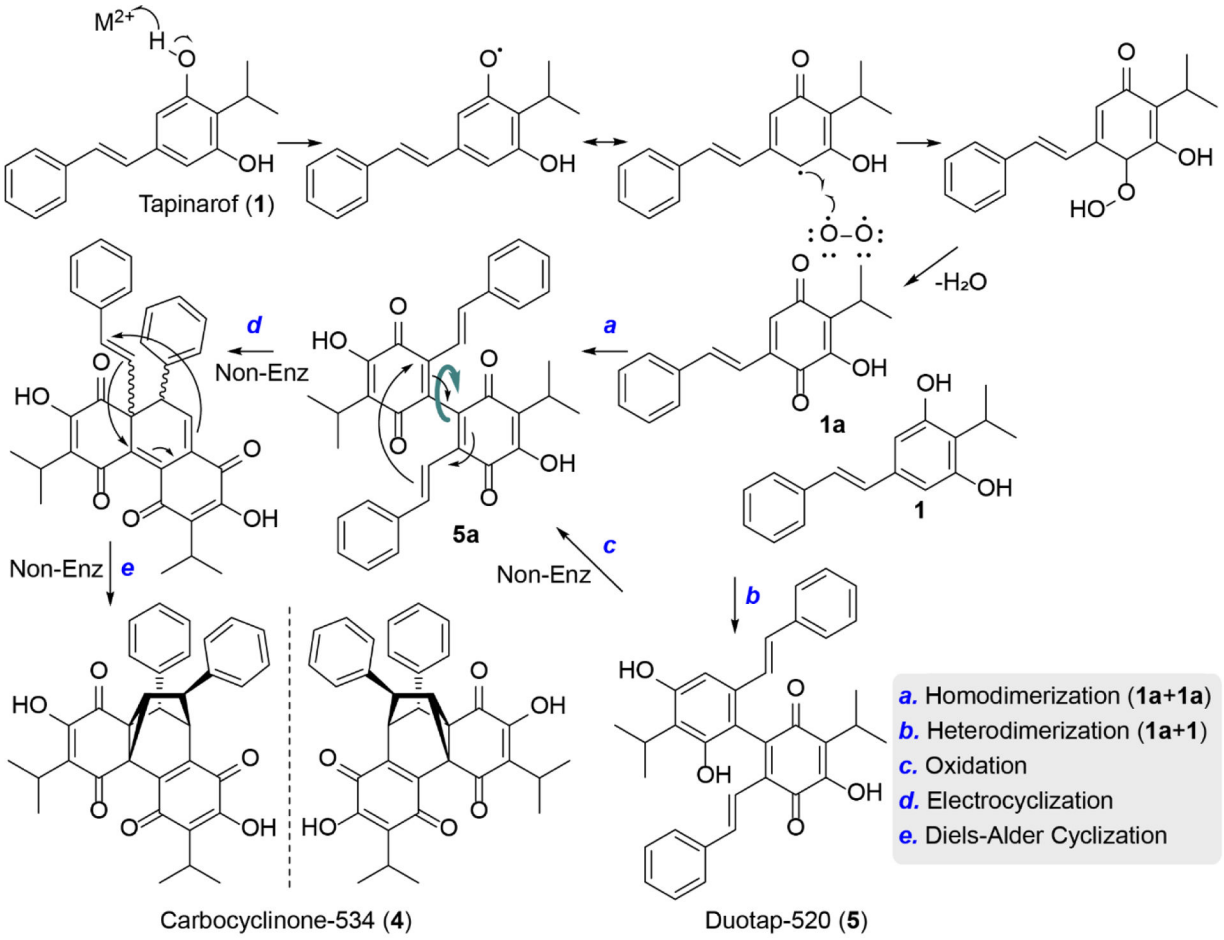

Figure 5.

Proposed pathway of carbocyclinone-534 (4) and duotap-520 (5) formation via regioselective dimerization of tapinarof (1).

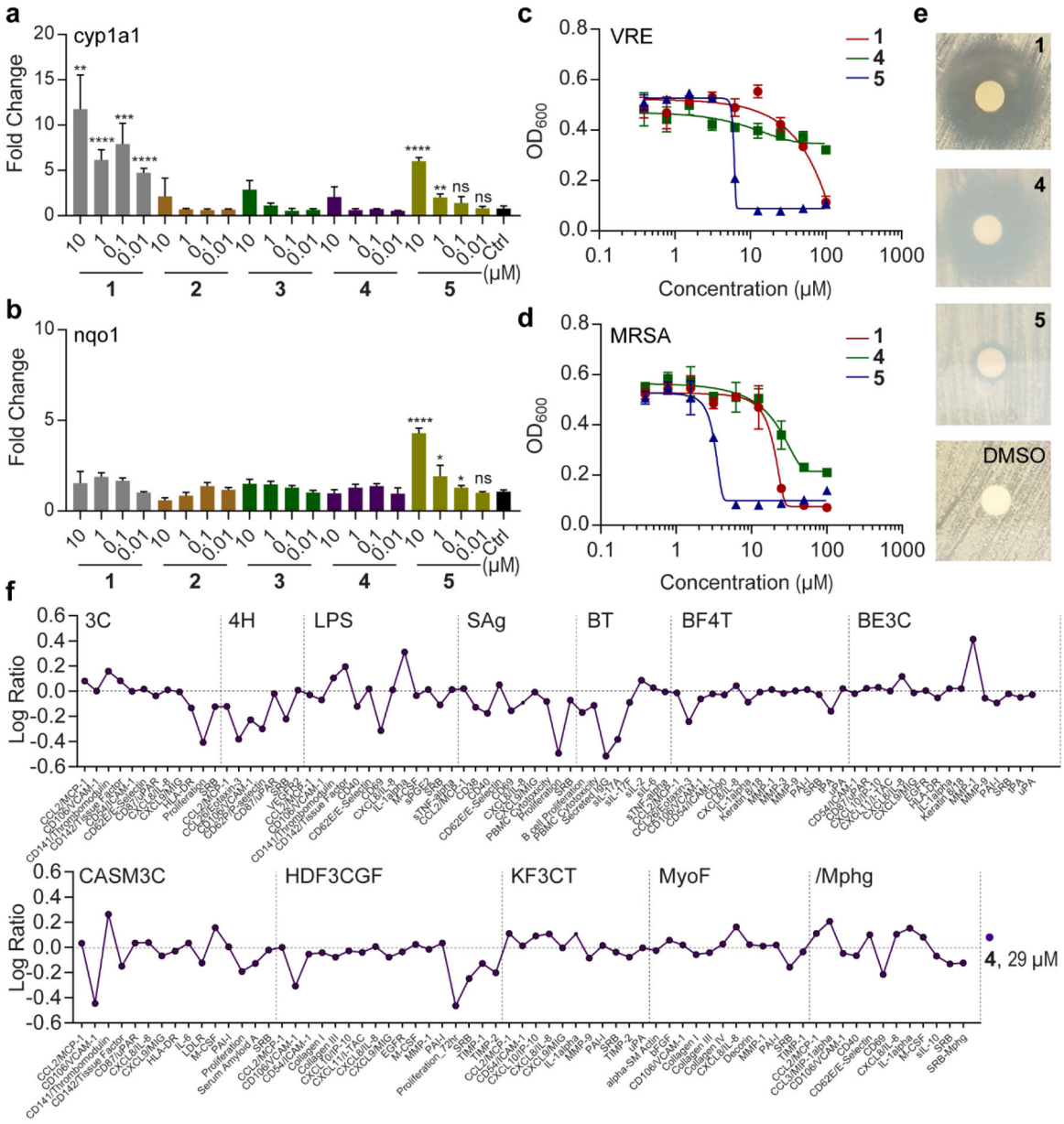

Figure 6. Bioactivity of tapinarof-derived metabolites.

a and **b**, Activation of *cyp1a1* and *nqo1* by metabolites in human Hct116 cells. The mean and SD of three biological replicates for each concentration are shown. **c** and **d**, Dose-response curves of metabolites against vancomycin-resistant *Enterococcus faecalis* (VRE) and methicillin-resistant *Staphylococcus aureus* (MRSA). The mean and SD of three independent replicates are shown. **e**, Disk diffusion assay to evaluate inhibitory activity of compounds against *Mycobacterium smegmatis* (100 μg compound/disk). **f**, BioMAP analysis of **4**.

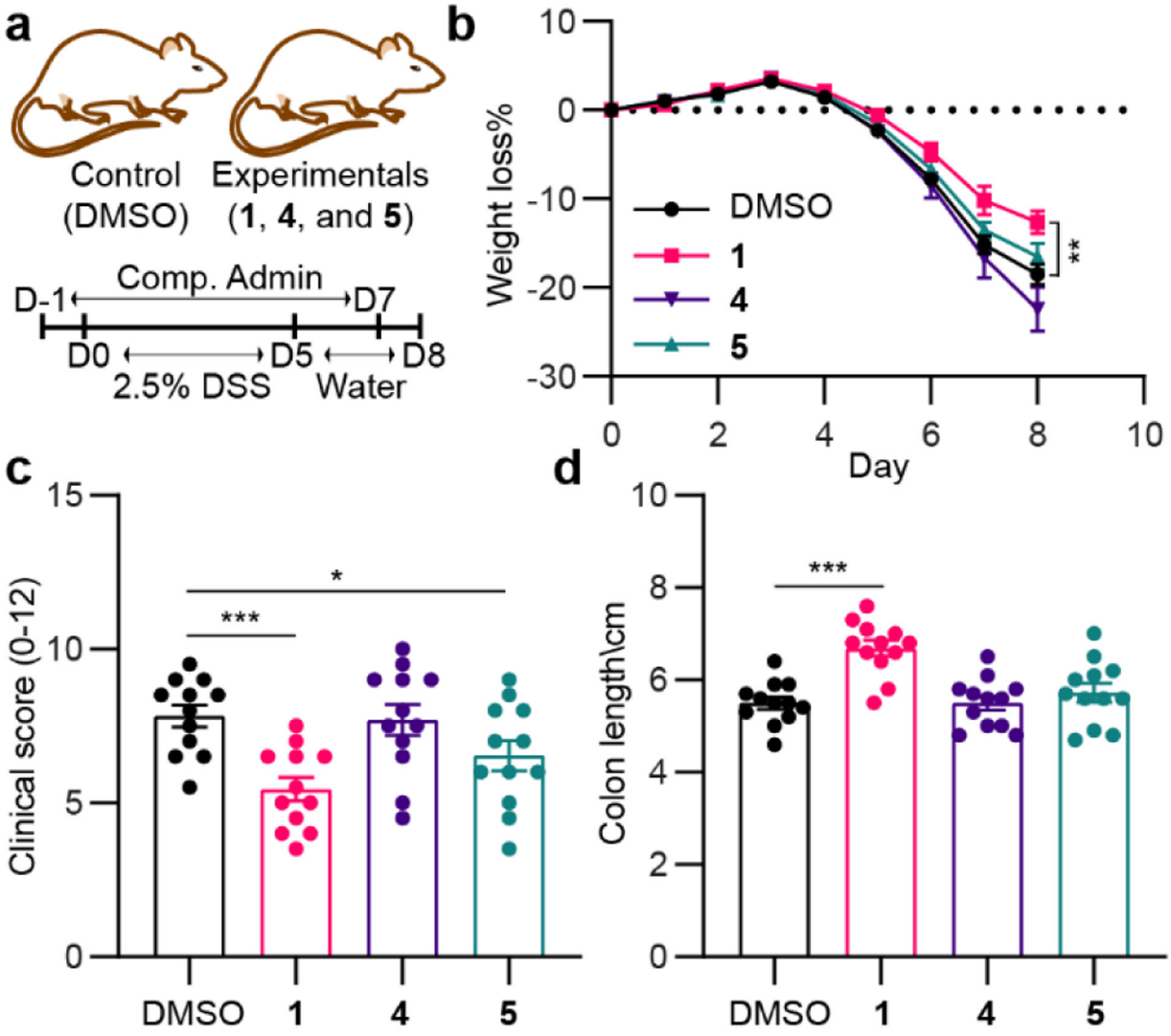

Figure 7. ***In vivo*** **study with metabolites 1, 4, and 5 in a colitis mouse model.**

a, Workflow for DSS (2.5%) and compound (5 mg/kg) administrations to C57BL/6 mice. **b**, Body weight loss of each mouse was depicted as the percentage (%) compared to the initial body weight. **c** and **d**, Endoscopy clinical scores (**c**) and colon length (**d**) of mice were measure at day 8. Statistical significance (two-tailed t-test) compared to control (DMSO): *P<0.05; **P<0.01; and ***P<0.001.